The Prediction of Ice Habit for Models: Influences on Mixed-Phase Cloud Glaciation

KARA J. SULIA[1,*], JERRY Y. HARRINGTON[1], AND HUGH MORRISON[2]

[1] *Department of Meteorology, Pennsylvania State University, University Park, PA*

[2] *National Center for Atmospheric Research, Boulder, CO*

1 Introduction

There is a critical need to improve parameterizations of cloud lifetime, for it can greatly impact the earth's energy budget, thus influencing climatic effects, namely in the Arctic. According to Francis and Hunter (2006), southerly winds, warm air advection from the south, downwelling long-wave flux (DLF), and downwelling solar flux (DSF) all may play a potential role in Arctic sea-ice decline. Among these, DLF shows the strongest correlation to the retreat of the sea-ice, and this increase in DLF is likely induced by increasing cloud-cover which effectively warms the surface. The correlations between clouds and sea-ice decline have also recently been investigated by Kay et al. (2008). During the summer of 2007, the Arctic sea-ice reached a record minimum extent. Kay et al. (2008) showed that decreased cloud-cover in summer months allowed the DSF to warm the ocean surface causing substantial ice melt. The warm open ocean induced evaporation, and cloud-formation resumed as winter set in. As polar night approaches, the effect of DLF dominates, and the ice surface again experiences a warming effect due to cloud cover (Francis and Hunter, 2006). These results suggest that the prediction of cloud-cover is critical for studies of sea-ice melt and Arctic climate as a whole.

Mixed-phase clouds are prevalent in the Arctic (e.g., Pinto, 1998), and the lifetime of these clouds exhibits a strong sensitivity to the number concentration and habit (shape) of the ice particles (Harrington et al., 1999). In such clouds, the growth by vapor deposition is significant, and so attention must be paid to how crystals evolve. Ice growth can not only lead to cloud glaciation, but may eventually lead to the stratus cloud dissipation and impact the climate effects discussed by Kay et al. (2008). For instance, Korolev and Isaac (2003) explore the effects of ice growth on the glaciation. They deduce that glaciation time, or the time it takes for ice to evaporate all liquid drops, is impacted by the environmental temperature (and thus supersaturation), updraft velocity, and ice number concentration. Their results indicate glaciation time is longer when the environmental temperature is warmer, $\sim -5^{\circ}C < T < -1^{\circ}C$ (and thus low saturation ratio), has a small initial ice concentration, and has either a higher updraft velocity or an oscillatory updraft. While the glaciation studies by Korolev and Isaac (2003) provide promising results, they only consider spherical ice particles, and state that non-spherical cases scale linearly with the capacitance in terms of the effect on cloud glaciation. However, non-spherical ice particle growth is non-linearly related to the change in aspect ratio (Chen and Lamb, 1994), and we find that non-spherical cases have a non-linear effect on glaciation time (see below).

Laboratory measurements show that crystal habit depends primarily on temperature, where plates exist in the temperature range $-10^{\circ}C < T < -22^{\circ}C$, columns in $-3^{\circ}C < T < -10^{\circ}C$ and $T < -22^{\circ}C$, and isometric growth dominates at the transition temperatures (Bailey and Hallett, 2009). Though these more "perfect" habits are found in the lab, many times crystals are irregular in atmospheric clouds (Korolev et al., 1999), most likely forming as polycrystals during drop freezing. Regardless of the final shape these crystals may acquire, the laboratory data provides us with information on the basic physics of how ice crystals grow. These non-isometric plates and columns can evolve into extreme habits such as dendrites and needles (respectively) at high (liquid) saturations. Chen and Lamb (1994) provide a successful model that captures the non-linear feedbacks between mass growth and habit evolution. We call this the 'Fickian-distribution'[1] model, as it describes how vapor diffuses toward the non-spherical crystals and how the vapor mass is distributed across the particle surface via the *mass redistribution hypothesis*. Sheridan et al. (2009) studies the non-linear feedbacks in growth using the Chen and Lamb (1994) model to examine cold cirrus. They find that initially smaller particles grow more quickly than initially larger particles, establishing a more pronounced habit, and as a result, can produce extreme aspect ratios. Larger particles do not experience such extreme effects.

Unfortunately, current cloud models inaccurately predict the

[*] *Corresponding author address*: K. J. Sulia, Department of Meteorology, Pennsylvania State University, 413 Walker Building, University Park, PA 16802; *e-mail*: kjs5066@psu.edu.

[1] The Chen and Lamb (1994) model is a modified 'capacitance' model, and has been re-termed the 'Fickian-distribution' model. This is because the analogy that compares the electrostatic potential existing around a charged conductor and a vapor density field surrounding an ice crystal, also known as the capacitance model, breaks down close to the surface of a non-spherical ice crystal. According to McDonald (1963), the capacitance model assumes that the vapor density surrounding the crystal is uniform everywhere, which is the case for isometric particles. This, however, is not the case for crystals with an aspect ratio different from unity or for faceted crystals. Moreover, the capacitance model holds the aspect ratio constant in time. The Chen and Lamb (1994) method improves this by using flux ratios from crystal growth theory.

growth of ice, assuming spheres or simple shapes. Avramov and Harrington (2010) show that the current method of calculating ice growth in models depends critically on assumptions made about crystal habit. Their results show that cloud cover can easily be made to vary from 0 to 100 % simply by the choice of crystal used in the model simulations. Fortunately, the ice growth problem is one that we can make progress on, and so we can improve the functionality of current cloud and climate models.

2 Vapor Depositional Growth and the Fickian-Distribution Model

Chen and Lamb (1994) developed a method for ice crystal growth from vapor that we term the Fickian-distribution model. Through Fick's Law, we know that the diffusion of vapor molecules toward the surface of an ice crystal is directly proportional to the vapor gradient at the particle edge. Isometric particles have the same gradient at all points on the crystal surface, thus, the flux of vapor toward the particle is the same in all directions, growing the crystal radially and uniformly. However, because non-isometric particles exist, the Fickian-distribution model helps us understand how varying fluxes over the principle crystal axes (a and c) influence crystal growth.

The fluxes over a spherical particle are given by Fick's Law as

$$F_v = \frac{D_v \Delta\rho_v}{r}, \tag{1}$$

where D_v is the vapor diffusivity, $\Delta\rho_v = \rho_{v\infty} - \rho_{vs}$ is the vapor density difference, and r is the particle radius. As the curvature ($\frac{1}{r}$) increases (radius decreases), the flow of vapor toward the particle surface rises. For the case of non-spherical particles in the capacitance model, these fluxes are modified as follows:

$$\begin{aligned} &Oblate(Plate): && Prolate(Column): \\ &F_a = \frac{D_v \Delta\rho_v}{c} f_{ob}(\phi) && F_a = \frac{D_v \Delta\rho_v}{c} \phi f_{pr}(\phi) \\ &F_c = \frac{D_v \Delta\rho_v}{a} f_{ob}(\phi) && F_c = \frac{D_v \Delta\rho_v}{a} \phi f_{pr}(\phi) \end{aligned} \tag{2}$$

where $\phi = \frac{c}{a}$ is the aspect ratio, and $f_{ob}(\phi)$ and $f_{pr}(\phi)$ are the respective oblate and prolate shape factors. F_a and F_c are the fluxes along the a and c-directions of the crystal, respectively. The above equations follow from the derivation of the capacitance of a spheroid, our proxy for non-spherical particles. Physically, these fluxes makes sense. For instance, consider a plate-like crystal (oblate), as the aspect ratio decreases for a constant volume, the a-axis length increases, and so the flux that grows c drops. As a consequence, one should expect faster growth of the a-axis (plate edges) and slower growth of the c-axis (plate basal face). However, in the capacitance model, the shape of the crystal evolves such that the aspect ratio remains constant in time. Classically, the capacitance model is given by (Pruppacher and Klett, 1997, pg. 547)

$$\frac{dm}{dt} = 4\pi C G_i (S_i - 1) \tag{3}$$

where

$$G_i = \left[\frac{L_s}{K_T T_\infty} \left(\frac{L_s}{R_v T_\infty} - 1 \right) + \frac{R_v T_\infty}{D_v e_i} \right]^{-1}$$

and

$$S_i = \frac{e_\infty}{e_i}.$$

Unlike the capacitance model, the Fickian-distribution model consists of Equation 2, the mass diffusion equation (3) above, and the *mass redistribution hypothesis* that derives from crystal growth theory (Chen and Lamb, 1994),

$$\frac{dc}{da} = \frac{\alpha_c F_c}{\alpha_a F_a} = \frac{\alpha_c}{\alpha_a} \phi = \Gamma\phi, \tag{4}$$

where α_c and α_a are the mass deposition coefficients along c and a, respectively. Central to the above hypothesis is the fact that Γ depends primarily on temperature (e.g., Chen and Lamb, 1994). *It is this hypothesis that makes the Chen and Lamb (1994) model fundamentally different from the capacitance model; this hypothesis allows the aspect ratio to evolve in time.*

The above hypothesis has some important consequences for aspect ratio evolution. To see this, consider the following analysis. Using the volume of a spheroid, it can be shown that $\frac{d\phi}{\phi} = \frac{dV}{V}\left(\frac{\Gamma-1}{\Gamma+2}\right)$. Combining with Equation 3 and assuming an initially small particle so that $C(a, c)$ is the radius, r,

$$\frac{d\phi}{\phi} \propto \frac{1}{r^2} \left(\frac{\Gamma - 1}{\Gamma + 2} \right). \tag{5}$$

Since $d\phi \propto \frac{1}{r^2}$, the smaller the initial radius of the crystal, the greater the change in aspect ratio. One of the physical consequences of the Chen and Lamb (1994) model is that more pronounced habits (either very large or small ϕ) should be produced for smaller initial ice crystals (e.g., Sheridan et al., 2009) leading to greater growth (see below).

It is also important to realize that there is a dependence of $d\phi$ on $\left(\frac{\Gamma-1}{\Gamma+2}\right)$ that is asymmetric with respect to shape. For instance, Sheridan et al. (2009) suggests that changing Γ symmetrically about $\Gamma = 1$ will lead to similar growth for the resulting plates ($\Gamma < 1$) or columns ($\Gamma > 1$). This, however, is not the case. As an example, consdier $\Gamma = 1 \pm 0.25$ for plates,

$$\left(\frac{\Gamma-1}{\Gamma+2}\right) = \left(\frac{0.75-1}{0.75+2}\right) = \left(\frac{-0.25}{2.75}\right)$$

and for columns,

$$\left(\frac{\Gamma-1}{\Gamma+2}\right) = \left(\frac{1.25-1}{1.25+2}\right) = \left(\frac{0.25}{3.25}\right).$$

The magnitude is greater for plates than for columns, suggesting faster growth of plates. However, given the same change in aspect ratio, columns will experience a greater change in $C(a, c)$ than plates. Thus, there is an asymmetry between the growth rate of plates and columns. As a result, columns grow more quickly when the same relative mass is deposited onto the crystals. In contrast, plates grow more quickly when the same change in aspect ratio ($d\phi$) is applied to the particles. Plates also grow more quickly when the same relative mass is deposited onto the crystals as long as they begin as spheres.

Current methods of ice particle growth as implemented into cloud models fails due to the fact that the nonlinear growth described above is not adequately captured. Therefore, the linear scaling to account for ice particle growth suggested by Korolev and Isaac (2003) is not sufficient and is an underestimation of actual crystal growth. The true nonlinearity in ice crystal growth can have significant effects on ice-containing clouds.

3 Box Model

3.1 Single-Particle Model

In order to understand the physicality embodied in Equations 3 and 5, or how mass and aspect ratio work in tandem to determine ice particle evolution, a box model is used. The box model is constructed to examine the growth of individual ice crystals, following Chen and Lamb (1994). First single-particle growth is used so that the reaction of a single particle to varying parameters, such as temperature and initial size, can be explored. Ice particle growth has a primary dependence on temperature through Γ, or the inherent growth ratio (hereafter termed IGR), so understanding how a particle grows at each temperature is critical for ice growth studies.

In our box model, all atmospheric parameters remain constant while particle size and aspect ratio evolve in time. Figure 1 is a comparison among Takahashi and Fukuta (1991) (black dots and circles), Chen and Lamb, 1994 (black lines), and box model results (red lines) at liquid saturation. The box model results are most comparable to both upper lines for the a and c-axes. These simulations were run allowing initially $1\,\mu m$ spherical particles to evolve for 20 minutes at each temperature in the range $-30^{\circ}C < T < -3^{\circ}C$. The box model results compare quite well to both the previous simulations and observational data, and even exhibit greater extremity at habit-prone temperatures.

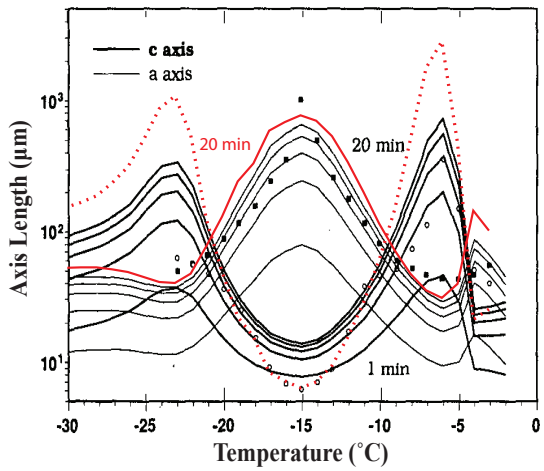

Figure 1: Comparison of Chen and Lamb (1994), their Figure 7 (black lines) with Takahashi and Fukuta (1991) data observations (black dots and circles) and box model results (red lines). Chen and Lamb (1994) show axes lengths of a single crystal after 1, 5, 10, 15, and 20 minutes of growth and includes ventilation, Takahashi and Fukuta (1991) show data after 10 minutes of growth, and box model results are after 20 minutes of growth without ventilation.

The initial spherical size of an ice particle can also have dramatic effects on the growth of crystals, predominantly at habit-prone temperatures. Figure 2 shows the mass after 20 minutes of growth for four different initial particle radii. Initially smaller particles attain larger final masses as compared to initially larger particles. In fact, initially larger particles have a final mass similar to that of a purely spherical particle. To explain this concept, we explore the relative change in mass of both small and large particles. This change depends on the ratio of the surface area to the volume of the particle:

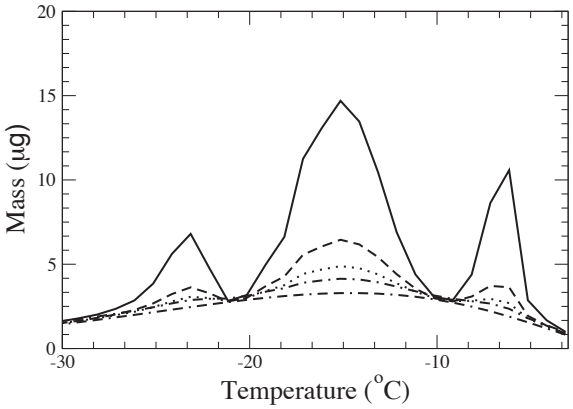

Figure 2: Particle mass with respect to temperature after 20 minutes of growth. Initial radii of $1\,\mu m$ (solid), $5\,\mu m$ (dashed), $10\,\mu m$ (dotted), and $20\,\mu m$ (dashed-dotted), are shown. We also show spherical growth for a $1\,\mu m$ initial particle size (dashed-dashed-dotted).

$$\frac{A_s}{V} = \frac{4\pi r_i^2}{\frac{4}{3}\pi r_i^3} = \frac{3}{r_i} \tag{6}$$

Because the ratio of the surface area to the volume of a sphere is inversely proportional to the radius, smaller spheres will have a larger area to volume ratio as compared to larger spheres. Consequently, a larger area to volume ratio for smaller ice spheres means that more relative mass is deposited as compared to larger spheres for the same vapor flux, as seen in Figure 3. Therefore, smaller particles grow more rapidly than larger particles.

3.2 Habit Influences on Ice Particle Distribution Evolution

The substantial effect of initial particle size on growth indicates that there could be more important consequences for the evolution of a distribution ice crystals. Expanding on Sheridan et al. (2009), we examine the impact of mass and aspect ratio evolution on a distribution of particles. Particles begin as spheres

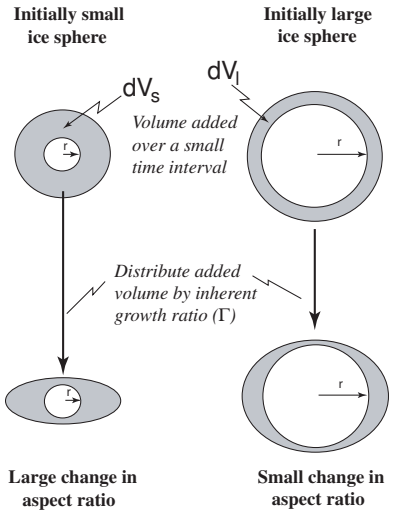

Figure 3: From Sheridan et al. (2009): Relative growth rate of initially smaller ice spheres as compared to initially larger ice spheres.

in the box model and evolve into non-spheres over 200 seconds (Figure 4). Calculations are completed for dendritic crystals ($-15^{\circ}C$) in a liquid saturated environment, enabling rapid growth. As the distribution evolves, the initially smaller particles catch up to and eventually grow larger than the initially larger particles (Figure 4a). In addition, as time progresses, the aspect ratio of all particles deviates more and more from unity with the initially smaller particles achieving the most extreme habits (Figure 4b).

The relative growth rates of distributions of ice particles and their dependence on initial size and environmental variables play a critical role in the glaciation time of simulated clouds. As expressed by Korolev and Isaac (2003), glaciation time depends primarily on temperature and ice concentration. If a large number of ice particles exist in a volume of cloud, this results in a large surface area onto which vapor can deposit. If the environment is at liquid saturation, a population of supercooled liquid drops is presumed to exist, and the ice particles will grow through vapor deposition at the expense of the liquid drops via the Wegener-Bergeron-Findeisen (hereafter Bergeron) process (Castellano et al., 2004). Assuming a constant concentration of liquid drops, a cloud that contains more ice particles will glaciate more quickly due to the Bergeron Process than a cloud with fewer ice particles.

What Korolev and Isaac (2003) do not include are the effects of habits on glaciation. As seen in Figure 2, crystal habits will attain a greater mass in certain temperature ranges than in others and so will have a larger impact on the vapor budget. Using spheres critically underestimates the glaciation time of clouds. Figure 5 gives us an idea of how glaciation time is affected by the critical parameters discussed above. As shown by Korolev and Isaac (2003), the glaciation time of a cloud is highly dependent on the ice concentration and it is clear from Figure 5 that this is indeed the case. Higher ice concentrations induce faster glaciation because there are more particles relative to the same liquid water content. Note that including the growth of non-spherical particles produces much shorter glaciation times, but that this influence also depends on concentration itself. For instance, our simulations show results closer to those of spherical particles when ice concentrations are high because the glaciation time is so rapid that these particles cannot establish an extreme habit. In addition, the initial particle size can have a critical effect on the glaciation time at habit-prone temperatures (and their relative IGR). In some cases (i.e., $N = 10^0\, L^{-1}$), ignoring habit can critically underestimate the glaciation time, by an order of magnitude in some cases. Note that the smaller the initial particle size, the more extreme the aspect ratio, and hence the faster the cloud can glaciate. This initial size effect is most pronounced at low concentrations seeing as glaciation times are long and ice particles have time to develop more extreme habits.

Many times, equivalent density spheres are used to approximate ice crystal growth. Figure 5 shows that this estimation is insufficient, particularly at low ice concentrations. The density of ice that deposits onto the particle over one time-step can be approximated as (Chen and Lamb, 1994):

$$\rho_{dep} = 920 \cdot exp[-3 \cdot max(\Delta\rho - 0.05, 0)/\Gamma(T)] \qquad (7)$$

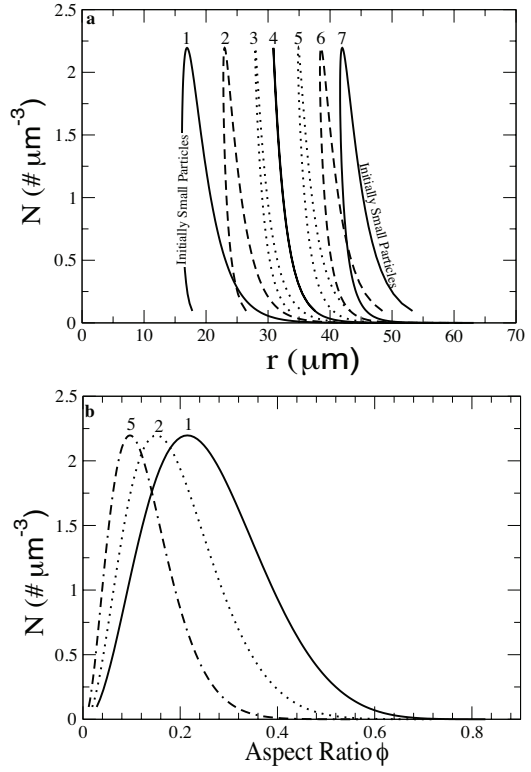

Figure 4: (a) Evolution of the size distribution of particles at a temperature of -15°C at liquid saturation. (a) Equivalent volume spherical radius (r) and (b) aspect ratio are shown. Line 1: time = 30s; Line 2: time = 60s; Line 3: 90s; Line 4: time = 110s; Line 5: time = 140s; Line 6: time = 170s; Line 7: time = 200s

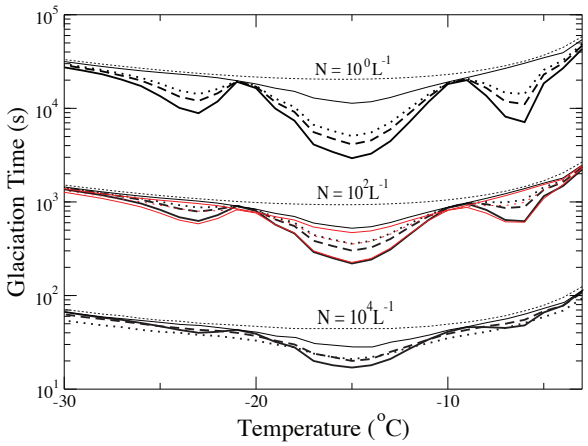

Figure 5: Glaciation time with respect to temperature for different initial ice concentrations for radii of $1\,\mu m$ (solid), $5\,\mu m$ (dashed), and $10\,\mu m$ (dotted). The thin solid line represents a spherical particle of equivalent density, the small dotted line represents a spherical particle with a constant density of $920\frac{g}{m^3}$, and the red lines are comparisons to Westbrook et al. (2008). Initial liquid water content is $0.2\frac{g}{kg}$.

where $\Delta\rho$ is the excess vapor density in $kg\,m^{-3}$. Secondary habits are parameterized by this deposition density. At liquid saturations (where $\Delta\rho_v$ is large), ρ_{dep} is small, thus accounting for the effectively lower density of dendrites and hollow columns. Accordingly for non-spherical particles, the deposition density is less than that of a spherical particle due to differing mass fluxes described by Equations 1 and 2. Therefore, the aspect ratio can become even more pronounced at high saturations leading to even greater growth of non-spherical particles as compares to spheres (Figure 5). The more pronounced habits occur when growth times are the longest, which is at the lowest ice concentrations. It is no wonder, then, that equivalent volume density spheres are a poor approximation of growth; however, this approximation improves when concentrations are high.

It is also important to note that the simulations above use a spheroid as a proxy for crystal growth. The red lines on Figure 5 shows results using the capacitance of a hexagonal plate as derived by Westbrook et al. (2008). As we can see from Figure 5, the spheroidal results compare quite well to the results of Westbrook et al. (2008), and thus we presume that a hexagonal prism can be approximated as a spheroid with sufficient accuracy.

In summary, the preceding analysis tells us the following: First, habit evolution is non-linear and cannot be accurately captured by equivalent density spheres because of the strong temperature dependence based on habit. This is especially true at low ice concentrations, which are typical of most mixed-phase clouds. However, spheres may work well where ice concentrations are relatively high ($\geq 10\,cm^{-3}$). Second, initially smaller spheres have a larger relative volume increase as compared to initially larger spheres, resulting in a larger change in aspect ratio. This larger aspect ratio change feeds into the capacitance term which then leads to faster growth of these initially smaller particles. As a consequence, an initial size-dependence for ice growth and mixed-phase glaciation appears.

4 Parcel Model

The above analysis provides a way for us to understand how a distribution of ice particles may behave in a more realistic cloud environment. We extend our analysis using a Lagrangian parcel model framework. The parcel model allows environmental variables such as temperature, pressure, and saturation to vary with time (and height). The parcel begins at a prescribed temperature, pressure, and in a slightly subsaturated (with respect to liquid) environment. As the parcel rises (according to a predetermined updraft velocity) and reaches liquid saturation, a distribution of liquid drops will form due to the swelling and growth of an initial CCN (cloud condensation nuclei) population, and an ice distribution will begin to grow via the Bergeron Process. The varying environmental parameters are solved with VODE (Variable Order Differential Equation Solver). To simplify the solution procedure, VODE solves equations for the equivalent volume spherical radius over a time-step with the a and c axis length influence on the shape factor held constant. It is then possible to estimate new values of a and c from the new radius.

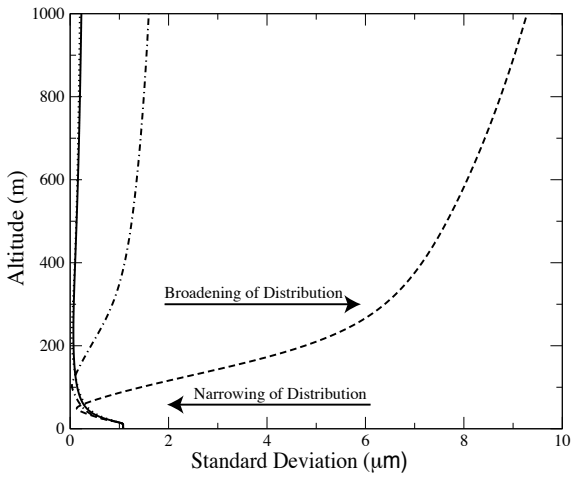

Figure 6: Standard deviation of particle radii distribution with respect to altitude. All initial distribution begin with and average radius of $2\,\mu m$. Simulations are run for 2000 seconds for an updraft velocity of $w = 0.5\,m\,s^{-1}$. Runs include base temperatures of $-10°C$ (dashed-dotted), $-15°C$ (dashed), $-20°C$ (solid), and $-30°C$ (dotted).

4.1 Constant Updraft Velocity: Ice Only

Because habit evolution depends primarily on temperature though the inherent growth ratio, Γ, it is important to under-

stand how particles grow in an environment where the temperature decreases with height.

Figure 6 shows the standard deviation of the particle radii distribution with respect to altitude. Note that the evolution of the distribution is highly dependent on initial parcel temperature. We know that rapid habit development and growth occurs at $-15^{\circ}C$ (dendrites, as indicated by the dashed line). As explained by Equation 1 and Figure 3, we know that smaller particles grow more quickly than larger particles and the effect that this has on a distribution (Figure 4a). We also know that at habit-prone temperatures, initially smaller particles achieve more extreme aspect ratios. Consequently, at $-15^{\circ}C$, very rapid particle growth occurs and the smallest particles in the distribution overtake the larger particles. This result is indicated first by a narrowing and then a broadening of the distribution. As altitude increases, the temperature of the parcel drops, the particles experience weaker growth, and the broadening of the distribution begins to ease. At temperatures $T < -24^{\circ}C$, habit growth is weakly prolate approaching nearly isometric. The initially smaller particles will accumulate more relative mass than the larger particles, but as they grow they do so more isometrically, and thus will have a shape nearly identical to the initially larger particles. As a result, the distribution will narrow, but the smaller particles will not outgrow the larger particles, preventing a broadening of the distribution. In the case where the initial temperature is $-10^{\circ}C$, all particles begin to grow nearly isometric (narrowing), but as the temperature drops and approaches that of significant habit growth, the distribution broadens slightly. We do not see the same pattern in distribution evolution in this case as we do for $-15^{\circ}C$ because the time when particles are most susceptible extreme habit development is when they are their smallest. Once the particles in the $-10^{\circ}C$ case reach $T \sim -15^{\circ}C$, they have accumulated mass isometrically and are now larger spheres. Hence, they do not develop extreme aspect ratios but grow as depicted in the right of Figure 3.

4.2 Constant Updraft Velocity: Liquid and Ice

Now that we have an understanding of how ice grows in an idealized parcel, we examine mixed-phase scenarios by introducing a population of liquid water droplets. As discussed previously, liquid drops grow continuously from an initial population of ammonium bisulfate aerosol via Köhler Theory. The vapor source for ice growth is controlled by the available liquid water content (LWC), which in turn is controlled by the environment in which the parcel resides. Understanding the interactions between liquid and ice in a parcel is important when determining the glaciation and overall lifetime of a cloud. For instance, Figure 7 shows the LWC and ice water content (IWC) for differing updraft speeds and initial ice concentrations. As expected, the parcels with the higher initial ice concentration glaciate more quickly than those with lower concentrations, and this is due in part to the larger surface area onto which vapor can deposit. Glaciation depends primarily on the available vapor in the environment, or the supersaturation, as described by

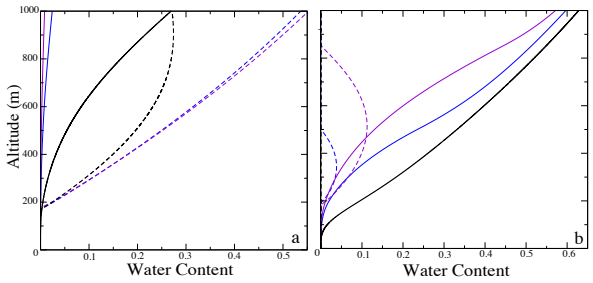

Figure 7: LWC (dashed) and IWC (solid) with respect to altitude at updraft velocities of $0.1\,m\,s^{-1}$ (black), $0.5\,m\,s^{-1}$ (blue), and $1.0\,m\,s^{-1}$ (violet) and initial ice number concentrations of (a) $1\,L^{-1}$ and (b) $50\,L^{-1}$.

(Korolev and Isaac, 2003):

$$\frac{dS}{dt} = Q_1 w - Q_2 \frac{d\omega_L}{dt} - Q_3 \frac{d\omega_I}{dt} \tag{8}$$

where $Q_1 w$ is the production of supersaturation resulting from adiabatic cooling and $Q_2 \frac{d\omega_L}{dt}$ and $Q_3 \frac{d\omega_I}{dt}$ are the consumption of supersaturation by the growth of liquid drops and ice particles, respectively. The updraft velocity is a great determinant in whether or not a cloud glaciates, for it is the source for supersaturation. The greater the updraft, the greater the supersaturation production rate, and thus, the greater the amount of available vapor. In a faster updraft, the drop and ice particle growth (sink terms) is weaker in a relative sense, and so the vapor supply is not rapidly depleted, thus keeping the saturation high. The IWC is greater for slower updraft velocities due to the fact that the source of supersaturation is weaker, which gives the ice particles greater opportunity to use up the available vapor causing the drops to evaporate in order to keep the environment supersaturated, thus glaciating the cloud. Just as in Figure 5, glaciation is highly dependent on temperature and initial particle size due to habit influences. In the case of the parcel model, glaciation time is reduced for initially smaller particles at habit-prone temperatures because of the particle's ability to take up vapor more rapidly than isometric particles.

4.3 Oscillating Updraft Velocity

Implementing an oscillating updraft artificially mimics the normal vertical motion fluctuations that occur in an actual cloud. A cosine function with a maximum speed of $0.5\,m\,s^{-1}$ is used to mimic both up and downdrafts. During ascent, secondary habits are estimated by the deposition density (for instance, dendrites have a lower effective density than a plate). Therefore, a method is required for removing an appropriate amount of mass from the crystal during descent when crystals sublimate. For example, when a dendrite enters a subsaturated region, only the tips of its branches begin to sublimate, and so the density of the sublimated ice is much less than that of bulk ice ($920\,kg\,m^{-3}$). Assuming the sublimation density of a solid particle for a non-spherical particle is a clear overestimation of sublimation mass, and therefore triggers premature depletion of the ice crystal. If the cloud has not yet glaciated, this can

lead to an overestimation of glaciation time, for the mass and overall surface area of ice is reduced. If the cloud has glaciated, the reduction of the ice population can significantly underestimate the lifetime of the cloud. Therefore, in order to accurately represent the subsaturation influences of the downdraft, a sublimation density is implemented to account for the mass density removed:

$$\rho_{sub} = \rho_{ice}[1 + \beta] \tag{9}$$

where $\beta = \frac{\rho_i}{\rho_{ice}(t)} \frac{1}{ln(\frac{V_o}{V_i})}$, $V_o = \frac{4}{3}\pi r_o^3$ is the initial crystal volume at the beginning of growth, and V_i and ρ_i are the initial volume and density of the crystal at the beginning of each time-step, respectively. This sublimation density can be used to find the crystal density after each time-step:

$$\rho_f = \rho_i \left(\frac{V_i}{V_f}\right) + \rho_{sub}\left[1 + \frac{V_i}{V_f}\right]. \tag{10}$$

As discussed by Korolev and Isaac (2003), an oscillating updraft lengthens the glaciation time of a cloud, especially when ice concentrations are low. At low concentrations the deposition rate cannot easily adapt to the rapid changes in supersaturation, so the environment remains supersaturated with respect to liquid and the cloud remains mixed-phase. We find that in addition to ice concentration, initial particle size and

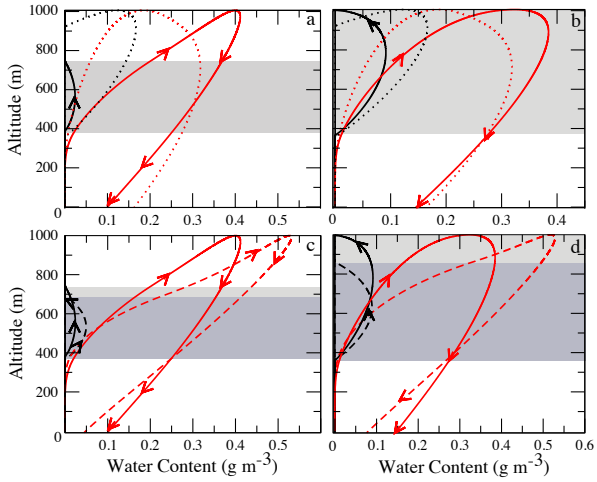

Figure 8: LWC (black) and IWC (red) with respect to altitude for an initial ice concentration of $N = 10\,L^{-1}$, initial particle radii of (a)/(c) $2\,\mu m$ and (b)/(d) $10\ \mu m$, and an oscillatory updraft with a maximum velocity of $0.5\,m\,s^{-1}$. Simulations for spheres (dotted), non-spheres with initial temperature $T = -10^{\circ}C$ (dashed) and $T = -15^{\circ}C$ (solid). Light grey represents mixed-phase regime for $T = -15^{\circ}C$, and dark grey for $T = -10^{\circ}C$. Glaciation occurs at altitudes above the mixed-phase regimes.

the inclusion of non-spherical particles also greatly impact the glaciation time of clouds (Figure 8). Figures 8a and 8b include non-spherical and spherical particles, indicating how these affect glaciation. Figure 8a uses an average initial radius of $2\,\mu m$ and 8b is that for a $10\,\mu m$ radius. The light grey shading represents the mixed-phase region for the non-spherical particles. It is clear from these images that glaciation for non-spherical particles occurs before spherical particles, and in the $2\,\mu m$ case, glaciation occurs quite a bit earlier. Figures 8c and 8d compares initial temperatures of $-10^{\circ}C$ and $-15^{\circ}C$ for initial radii of (c) $2\,\mu m$ and (d) $10\ \mu m$. The mixed-phase regimes are dark grey and light grey for $-15^{\circ}C$ and $-10^{\circ}C$, respectively. These figures show that even at the transition temperatures where particles grow nearly isometrically, assuming spherical particle growth would produce a clear underestimation of glaciation due to the fact that the particles are advected into regions with other temperatures which then affects their growth.

5 Bulk Microphysical Paramterization

The results from the box and Lagrangian parcel model simulations indicate a number of things about predicting crystal habit which are important for any model simulation of mixed-phase clouds. Of all the results discussed above, two are most important when it comes to predicting the overall mass evolution of ice within a mixed-phase cloud: (1) Aspect ratio and (2) crystal density. As shown above, equivalent density spheres are not a sufficient proxy for estimates of ice crystal mass evolution except at the transition temperatures between habits. Consequently, predicting a single axis length, or an equivalent radius is not sufficient primarily because non-linear feedbacks between crystal aspect ratio and crystal mass are not accounted for. Crystal density is vital as it is the only possible way to deal with low density habits like dendrites. Any model parameterization of ice crystal growth should attempt to capture the two processes enumerated above.

5.1 Methodology

The goal of the bulk microphysical model is to minimize computation time as much as possible without sacrificing the core physicality. This is accomplished by predicting only the essentials, and deriving other necessary variables associated with the habitual growth from these essentials. We propose a method that evolves a bulk distribution of crystal mass, aspect ratio, and effective density over time. Bulk models naturally involve a number of assumptions, and our first core assumption is that ice concentration is distributed over the a-axis length. The second core assumption we make is that the a and c-axes are related historically. The historical relation is derived directly from mass distribution hypothesis give by Equation 4. With these two assumptions, it is then possible for us to predict an a-axis mixing ratio (or a mean a-axis length) only, and derive the c-axis mixing ratio (or mean c-axis) length from the historical relation. In order for us to predict the evolution of the ice water content and the mean axis lengths, only a few predictive variables are required: The mass mixing ratio, the a-axis length, the historical aspect ratio, and the crystal effective density. Consequently, rather than predicting two variables, as is traditional in most two-moment bulk microphysical models, we require the prediction of four variables. However, this is a vast improvement over methods such as Chen (1992) in which

a two-dimensional distribution of a and c are tracked. Unlike that complex method, our method is relatively accurate (as we show below), and is computationally expedient making it amenable to bulk microphsyical modeling. The mathematics behind the method are rather involved, and for brevity they are not repeated here.

5.2 Comparison to Detailed Model

We compared our new bulk method with an accurate numerical solution to the Chen and Lamb (1994) model. Tests were done with two frameworks. First, we tested the bulk model using a box model framework. We mimic temperature changes by simply specifying an effective lapse rate and updraft speed. These initial tests were conducted in order to test the primary physicality of the model. Figure 9 shows that the preliminary

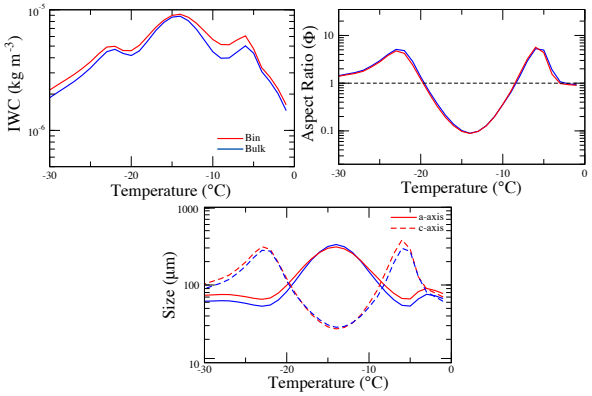

Figure 9: Evolution of IWC, aspect ratio, and a and c-axis lengths with respect to temperature. Bin model (red) and bulk model (blue) runs completed for initial average radius of $10\,\mu m$, $N_i = 1\,L^{-1}$, $w = 0.5\,m\,s^{-1}$, $\rho_i = 920\,kg\,m^{-3}$, and $\frac{dT}{dz} = -6.5\,K\,km^{-1}$ for 30 minutes.

bulk model runs compare extremely well with the detailed bin model. Ice water content, mean a and c-axis lengths, and mean aspect ratio are all well-predicted for the distribution after 30 minutes of growth. This comparison gives us confidence that the core of the bulk model is constructed accurately and contains the main physics we hope to reproduce in a cloud model.

A more robust set of tests were conducted next. In these tests, we implemented our bulk model into the same parcel framework used by our Lagrangian-bin version of Chen and Lamb (1994). These tests are more robust because temperature, pressure, and saturation state all change in time. Simulations like those shown in Figure 8 were completed using the bulk model and are shown on Figure 10. As is readily evident, the bulk-parcel model compares astonishingly well to the detailed parcel model with slight mass and size discrepancies in the downdraft. It is assumed that this error is due to the fact that the distribution shape is allowed to transform over time in the detailed parcel model, however, the distribution shape remains constant in the bulk model. In other words, the behavior described by Figure 4 cannot occur in a bulk model. Because the

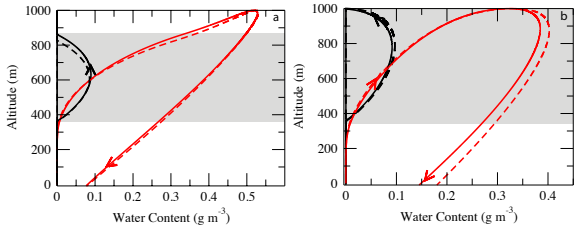

Figure 10: LWC (black) and IWC (red) with respect to altitude for an initial ice concentration of $N = 10\,L^{-1}$, initial particle radius of $10\,\mu m$, and an oscillatory updraft with a maximum velocity of $0.5\,m\,s^{-1}$. Simulations for detailed parcel (solid) and detailed bulk (dashed). The shaded region represents the mixed-phase regime for (a) $T = -10°C$ and (b) $T = -15°C$. Glaciation occurs at altitudes above the mixed-phase regimes.

(characteristic) masses and sizes of the particles in both models depend on the shape of the distribution, or ν, it is understood why slight differences between the bulk and detailed models occur.

Figures 9 and 10 are promising results and indicate that the bulk model we have constructed not only maintains the core physicality, but exhibits accurate results as compared to the detailed Lagrangian model.

6 Kinematic Model

The successful testing of the bulk model against the detailed Lagrangian parcel model lead us to further test the method through implementation into the two-dimensional (2D) kinematic model described by Morrison and Grabowski (2007, 2008, 2010). The kinematic model employs a specified flow field in a Eulerian framework, which allows for the testing of the microphysical scheme in a fashion that includes advective transport and particle sedimentation, while at the same time, avoiding complications due to feedbacks between the dynamics and microphysics.

6.1 Methodology

The kinematic model simulations occur in a Eulerian framework. Transport in physical space is calculated using the 2D version of the multidimensional positive definite advection transport algorithm (Smolarkiewicz and Margolin, 1998). The specified flow field varies in time, representing the evolution of an idealized shallow convective plume. The flow pattern consists of low-level convergence, upper-level divergence, and a narrow updraft at the center of the domain. Horizontal flow includes weak vertical shear, and the updraft velocity increases from rest to a maximum of $8\,m\,s^{-1}$ then subsequently decreases. The initial sounding for the case follows from Morrison and Grabowski (2010).

The bulk ice microphysics scheme developed for implementation into the Eulerian framework initializes ice via deposition and condensation-freezing as a function of ice supersaturation following Meyers et al. (1992). The method utilizes three of the

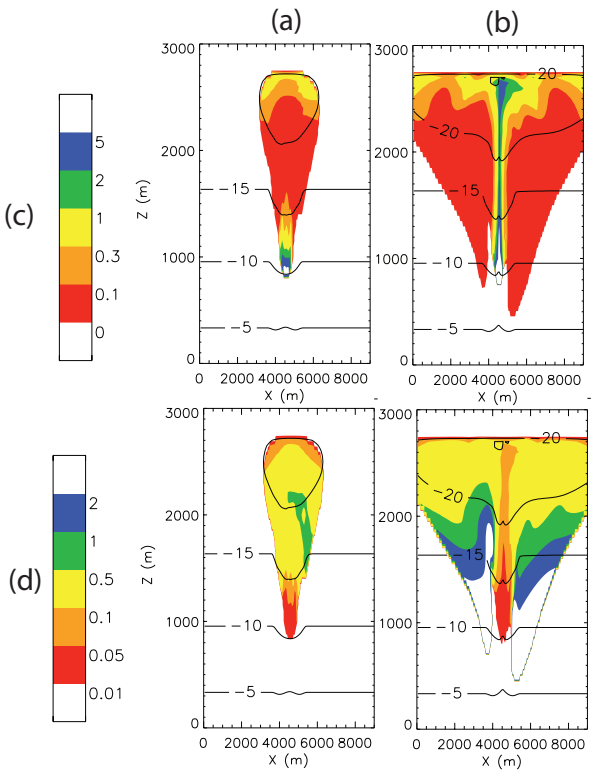

Figure 11: 2D fields for (respective rows) (c) aspect ratio, ϕ and (d) average a-axis length (mm) with superimposed contours of air temperature in degrees Celsius. Simulations are run for (a) 20 and (b) 30 minutes (respective columns). The cloud top temperature is approximately $-22^{\circ}C$, and the near-surface temperature is approximately $-3^{\circ}C$. Initial spherical particle radius is $1\,\mu m$.

four conserved prognostic variables used in the 'bulk-parcel' model: total ice number concentration, N_i, total ice mixing ratio, q_i, and bulk a-axis length mixing ratio. These three variables allow for the local derivation of potential temperature and water vapor mixing ratio, along with relevant quantities needed to calculate vapor deposition and sublimation, including the derivation of habit characteristics such as the aspect ratio, ϕ. Future work will include prediction of both bulk a-axis and c-axis length mixing ratios, allowing for the variable ice density discussed previously.

It is important to note that in the current implementation, aggregation has been neglected. For simplicity, we have also neglected liquid and mixed-phase microphysical processes, including freezing, riming, and melting. Again, the detailed mathematics is omitted to avoid verbosity.

6.2 Results

As seen in Figure 11, the cloud forms and grows as the updraft (located in the center of the domain) increases in strength. It reaches a maximum of $8\,m\,s^{-1}$ 25 minutes into the simulation, and then decreases. Initially, the particles nucleate and grow in the plate/dendrite regime around $-15^{\circ}C$ and have small values of $\phi < 0.1$ (not shown). As the cloud base decreases due to moistening over time, more crystals begin to nucleate and grow lower in the domain at temperatures $> -10^{\circ}C$ in the columnar regime, and have $\phi > 5$, as shown in 11a. These crystals are then carried upward in the updraft and at the top of the updraft between 2000 and $2500\,m$ where they spread out horizontally with the 2D flow and fall out through sedimentation on either side of the updraft, as shown in 11b. These crystals also grow further in the plate/dendrite regime between -10 and $-20^{\circ}C$ as they fall, and thus have small values of ϕ. There is also size-sorting of these particles, resulting in large a-mean axis length $> 2\,mm$ at the lower levels.

It is clear that the bulk microphysical model, adapted from the detailed parcel model, can be efficiently implemented into a Eulerian Model. This model accurately grows spherical ice particles into non-spherical habits through a simulated convective plume. We now see how the effects of advection and sublimation can impact the growth of these crystals. We hope to extend our studies to simulating mixed-phase clouds, and eventually predicting the habit effects of glaciation in such a model.

Acknowledgments. K. Sulia and J. Harrington would like to thank the National Science Foundation for support under grant ATM-0639542. Contributions from H. Morrison were supported by NOAA grant NA08OAR4310543, U. S. DOE ARM DE-FG02-08ER64574, and the NSF Science and Technology Center for Multiscale Modeling of Atmospheric Processes (CMMAP), managed by Colorado State University under cooperative agreement ATM-0425247.

References

Avramov, A. and J. Harrington, 2010: Influence of parameterized ice habit on simulated mixed phase arctic clouds. *J. Geophys. Res.*, **115**.

Bailey, M. P. and J. Hallett, 2009: A comprehensive habit diagram for atmospheric ice crystals: Confirmation from the laboratory, airs ii, and other field studies. *J. Atmos. Sci.*, **66**, 2888–2899.

Castellano, N., E. Avila, and C. Saunders, 2004: Theoretical model of the bergeron-findeisen mechanism of ice crystal growth in clouds. *Atmos. Environ.*, **38**, 6751–6761.

Chen, J., 1992: Numerical simulation of the redistribution of atmospheric trace chemicals through cloud processes. Ph.D. thesis, The Pennsylvania State University, University Park, PA, 16802, 342pp.

Chen, J. and D. Lamb, 1994: The theoretical basis for the parameterization of ice crystal habits: Growth by vapor deposition. *J. Atmos. Sci.*, **51 (9)**, 1206–1221.

Francis, J. and E. Hunter, 2006: New insight into the disappearing arctic sea ice. *EOS-Trans, AGU*, **87 (46)**, 509–524.

Harrington, J., T. Reisin, W. Cotton, and S. Kreidenweis, 1999: Cloud resolving simulations of arctic stratus, part ii: Transition-season clouds. *Atmos. Res.*, **51**, 45–75.

Kay, J., T. L'Ecuyer, A. Gettelman, G. Stephens, and C. O'Dell, 2008: The contribution of clous and radiation anomalies to the 2007 arctic sea ice extent minimum. *Geophys. Res. Let.*, **35 (L08503)**.

Korolev, A. and G. Isaac, 2003: Phase transformation of mixed-phase clouds. *Quart. J. Roy. Meteor. Soc.*, **129**, 19–38.

Korolev, A., J. Strapp, and G. Isaac, 1999: In situ measurements of effective diameter and effective droplet number concentration. *Quart. J. Roy. Meteor. Soc.*, **27**, 3993–4003.

McDonald, J., 1963: Use of the electrostatic analogy in studies of ice crystal growth. *Z. Angew. Math. Phys.*, **14**, 610–620.

Meyers, M., P. DeMott, and W. Cotton, 1992: New primary ice nucleation parameterizations in an explicit cloud model. *J. Appl. Meteor.*, **31**, 708–721.

Morrison, H. and W. Grabowski, 2007: Comparison of bulk and bin warm rain microphysics models using a kinematic framework. *J. Atmos. Sci.*, **64**, 2839–2861.

Morrison, H. and W. Grabowski, 2008: A novel approach for representing ice microphysics in models: Description and tests using a kinematic framework. *J. Atmos. Sci.*, **67**, 1337–1360.

Morrison, H. and W. Grabowski, 2010: An improved representation of rimed snow and conversion to graupel in a multicomponent bin microphysics scheme. *J. Atmos. Sci.*, in Press.

Pinto, J., 1998: Autumnal mixed-phase cloudy boundary layers in the arctic. *J. Atmos. Sci.*, **55**, 2016–2038.

Pruppacher, H. and J. Klett, 1997: *Microphysics of Clouds and Precipitation*. Kluwer Academic Publishers, Boston, 954pp pp.

Sheridan, L., J. Harrington, D. Lamb, and K. Sulia, 2009: Influence of ice crystal aspect ratio on the evolution of ice size spectra during vapor depositional growth. *J. Atmos. Sci.*, **66**, 3732–3743.

Smolarkiewicz, P. and L. Margolin, 1998: MPDATA: A finite-difference solver for geophysical flows. *J. Comput. Phys.*, **140**, 459–480.

Takahashi, T. and N. Fukuta, 1991: Supercooled cloud tunnel studies on the growth of snow crystals between -4 and -20°c. *J. Meteor. Soc. Japan*, **66**, 841–855.

Westbrook, C., R. Hogan, and A. Illingworth, 2008: The capacitance of pristine ice crystals and aggregate snowflakes. *J. Atmos. Sci.*, **65**, 206–219.